JACS
JOURNAL OF THE AMERICAN CHEMICAL SOCIETY

Article

pubs.acs.org/JACS

Inclusion Compound Based Approach to Arrays of Artificial Dipolar Molecular Rotors. A Surface Inclusion

Lukáš Kobr,[†] Ke Zhao,[‡] Yongqiang Shen,[‡] Angiolina Comotti,[§] Silvia Bracco,[§] Richard K. Shoemaker,[†] Piero Sozzani,[§] Noel A. Clark,[‡] John C. Price,[‡] Charles T. Rogers,[‡] and Josef Michl*[,†,∥]

[†]Department of Chemistry and Biochemistry and [‡]Department of Physics, University of Colorado, Boulder, Colorado 80309, United States

[§]Department of Materials Science, University of Milan—Bicocca, Italy

[∥]Institute of Organic Chemistry and Biochemistry, Academy of Sciences of the Czech Republic, 16610 Prague 6, Czech Republic

Supporting Information

ABSTRACT: We describe an approach to regular triangular arrays of dipolar molecular rotors based on insertion of dipolar rotator carrying shafts as guests into channels of a host, tris(*o*-phenylenedioxy)cyclotriphosphazene (TPP). The rotor guests can either enter the bulk of the host or stay at or near the surface, if a suitable stopper is installed at the end of the shaft. Differential scanning calorimetry, solid-state NMR, and powder X-ray diffraction were used to examine the insertion of a dipolar rotor synthesized for the purpose, 1-*n*-hexadecyl-12-(2,3-dichlorophenyl)-*p*-dicarba-*closo*-dodecaborane, and it was found that it forms a surface inclusion compound. Rotational barriers from 1.2 to 9 kcal/mol were found by dielectric spectroscopy and were attributed to rotors inserted into the surface to different degrees, some rubbing the surface as they turn.

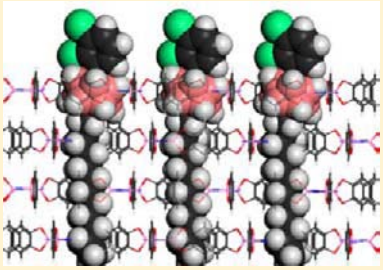

INTRODUCTION

Artificial molecular rotors promise access to ultrafast organic dielectrics useful for electronics, sensing, energy harvesting, and elsewhere, and a vast literature on the subject has been reviewed repeatedly.[1−7] Most have been examined in liquid solution, where they tumble and rotate randomly and independently, but it would be desirable to assemble rotors into two-dimensional (2-D) or three-dimensional (3-D) arrays.

In neat crystals of molecular rotors, the rotating parts (rotators) are oriented and separated as dictated by the bulk and intrinsic symmetry of the whole rotor molecule.[2] Many 3-D arrays of mostly nonpolar rotors have been studied within crystals,[8−12] and barriers as low as 1.5 kcal/mol have been engineered.[13] Many rotors located on surfaces have also been investigated over the years,[1] either as single molecules[14−20] or as collections of independently behaving molecules.[21−27] In all these assemblies, intermolecular interactions were weak and the motions of adjacent rotors uncorrelated.[28]

We are interested in designing rotor assemblies whose ground state is ferroelectric (dipoles of all rotators are aligned). This might be achieved in triangular lattices[29] of strongly coupled rotors with a very low rotational barrier. Engineering this in a neat crystal is very challenging. We use host−guest inclusion compounds, leaving the control of rotator orientation and separation up to the host and focusing the design of the rotator guest on achieving a large dipole and a low intrinsic barrier to rotation. The rotators could be inserted either at the surfaces of the porous crystalline host to produce a 2-D array or within its bulk to produce a 3-D array.

We report initial results obtained with hexagonal tris(*o*-phenylenedioxy)cyclotriphosphazene (TPP) as the host. Its layered structure, with a repeat distance of ∼5 Å, contains an array of parallel hollow channels separated by ∼11.5 Å, running perpendicular to the layers and forming a triangular lattice at intersections with them.[30−33] Their internal shape is not round but locally triangular, with the triangles rotated by 60° between adjacent layers (Figure 1). The channels are known to include a wide range of small molecular guests, from benzene to alkanes. Numerous inclusion compounds of TPP have been examined in the past, primarily by X-ray diffraction and solid-state NMR spectroscopy.[34−43] The ring currents of TPP benzene rings modify the chemical shifts of the nuclei of the guests by several ppm, allowing an inclusion to be readily recognized.

A complicating feature of TPP is the existence of a monoclinic modification,[35,38] incapable of forming inclusion compounds, and actually more stable than the hexagonal form containing empty channels. Filling the hexagonal TPP host with a nonvolatile guest makes it more resistant to transformation into the monoclinic form up to temperatures above 350 °C.[37]

A bulk inclusion of a rod-shaped molecule carrying a rotatable transverse dipole moment would provide a 3-D array that is regular except for a possible lack of registry of rotators contained in adjacent channels. If the rodlike guest molecule were prevented by a bulge in its shape (a "stopper") from inserting fully, it might form a regular 2-D surface inclusion, with a rotator just outside or just inside the surface of the solid.

Received: March 6, 2012
Published: June 1, 2012

   dx.doi.org/10.1021/ja302173y | *J. Am. Chem. Soc.* 2012, 134, 10122−10131

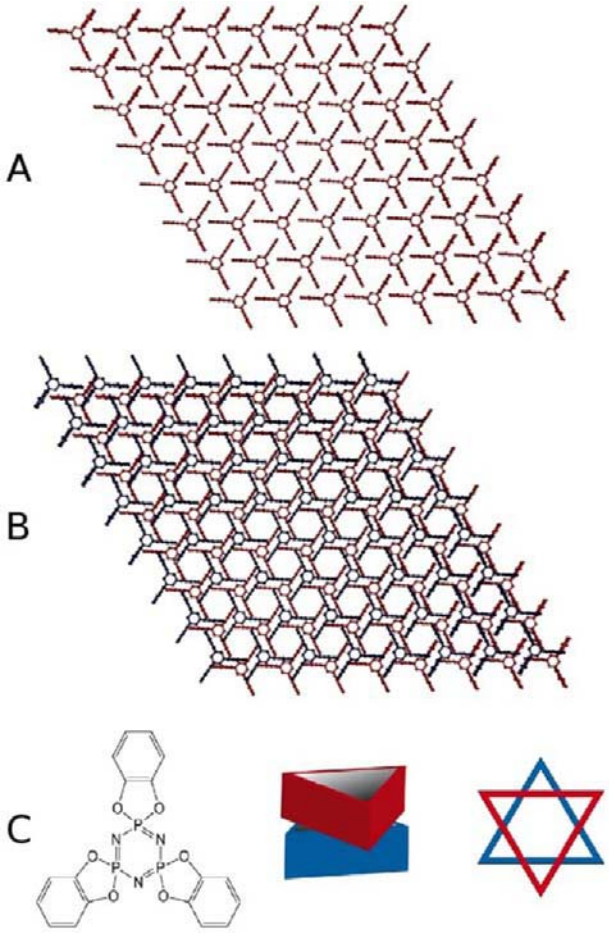

Figure 1. Crystal structure of TPP. Top view of a layer (A) and of two successive layers (B). Molecular structure, and schematic perspective and top views of the hollow channel (C).

Our rotor is 1-*n*-hexadecyl-12-(2,3-dichlorophenyl)-*p*-dicarba-*closo*-dodecaborane (**1** in Scheme 1), whose alkyl chain is designed to be the shaft, the icosahedral carborane the stopper, and the dichlorobenzene ring the dipolar rotator.

RESULTS

We describe the synthesis of **1**, assignment of ^{1}H and ^{13}C peaks in its liquid NMR spectrum, formation of an inclusion compound with microcrystalline TPP and its characterization by differential scanning calorimetry (DSC) and X-ray powder diffraction, analysis of the solid-state NMR spectra of **1** and its inclusion compounds, examination of their dielectric behavior, and calculation of the intrinsic rotational barrier in a model structure.

Synthesis (Scheme 1). Deprotonation of 1-triphenylsilyl-*p*-carborane (**2**)[44] with *n*-BuLi followed by alkylation with 1-*n*-hexadecyl bromide gave 1-hexadecyl-12-triphenylsilyl-*p*-carborane (**3**) in 90% yield. Deprotection with TBAF in THF afforded 1-hexadecyl-*p*-carborane (**4**) in 92% yield. Deprotonation and transmetalation with CuCl in the presence of pyridine, followed by Ulmann coupling with 1,2-dichloro-3-iodobenzene, afforded **1** in 92% yield.

TPP-d_{12} was prepared from 1,1,3,3,5,5-hexachlorocyclotriphosphazene and catechol-d_6,[45] obtained from catechol with H_2 and Pt/C in D_2O in isotopic purity better than 99.8% (by NMR), following a slightly modified literature procedure.[46] The deuteration was repeated twice, and purification of the perdeuterated product by chromatography on silica gel was avoided, since it induces H−D exchange.

Solution ^{1}H and ^{13}C NMR of 1. The NMR signals of **1** were assigned using ^{1}H−^{1}H gCOSY (Supporting Information (SI) Figure S1, top), ^{1}H−^{13}C gHSQC (Figure S1, bottom), ^{1}H NMR, boron-decoupled ^{1}H−^{13}C gHMBC NMR (J = 8 Hz, Figure S2 top; J = 18 Hz, Figure S2 bottom), ^{13}C NMR, and DEPT-135 (Figure 2) spectra, using standard procedures described in the Supporting Information. The assignments are summarized in Table 1. The ^{13}C signals at δ 10−40 ppm are due to the carbon atoms of the shaft, the two signals near δ 80−85 ppm to the carbons of the carborane stopper, and those at δ 120−140 ppm to the carbons of the rotator.

Solid-State ^{13}C CP MAS NMR of Neat 1 (Figure 2). The spectrum obtained with a long contact time t_C = 5 ms is similar to the solution spectrum, but the peaks are broader. The shift of the alkyl signal to 33.56 ppm from the solution value centered at 29.78 ppm is attributed to an all-anti conformation in the neat solid, contrasting with the presence of conformations containing one or more gauche twists in solution.[47] The C_i, C_j, and C_k carbon peaks in **1** are well separated and all similarly shifted 2−3 ppm upfield relative to the solution, while the *p*-carborane carbon signals are at nearly the same location in both spectra. In the aromatic region, the ^{13}C CP MAS spectrum displays several partially resolved resonances. They were grouped into those of protonated and of quaternary carbons by comparison with the solution spectrum and confirmed by a spectrum measured at t_C = 0.2 ms, in which quaternary carbon signal intensities are diminished.

Formation and DSC of Inclusion Compounds 1@TPP. Three inclusion compounds of **1** in TPP-d_{12} at concentrations of 8, 10, and 15 mol % were prepared by ball milling and annealing and are referred to as 8%**1**@TPP-d_{12}, 10%**1**@TPP-d_{12}, and 15%**1**@TPP-d_{12}, respectively.

Scheme 1. Synthesis of 1

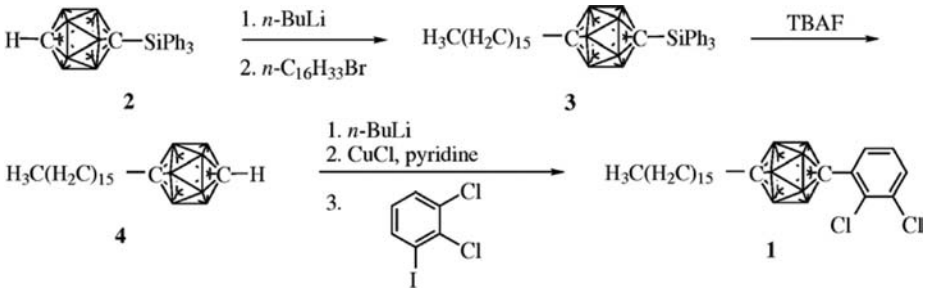

dx.doi.org/10.1021/ja302173y | J. Am. Chem. Soc. 2012, 134, 10122−10131

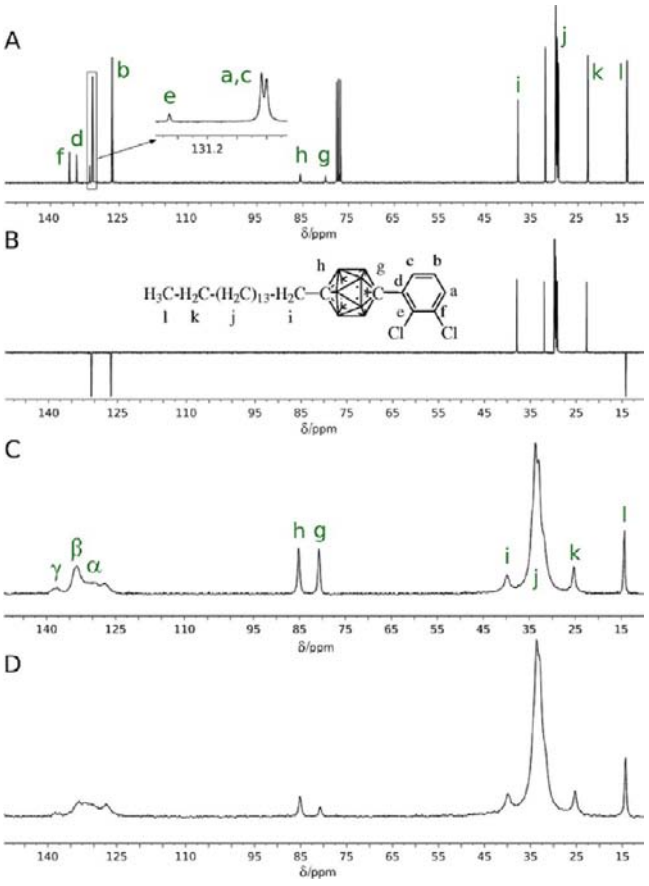

Figure 2. NMR spectra of rotor **1**. (A) ^{13}C NMR in $CDCl_3$ solution; (B) DEPT-135 in $CDCl_3$ solution; (C) t_C = 5 ms and (D) t_C = 0.2 ms solid-state ^{13}C CP MAS NMR.

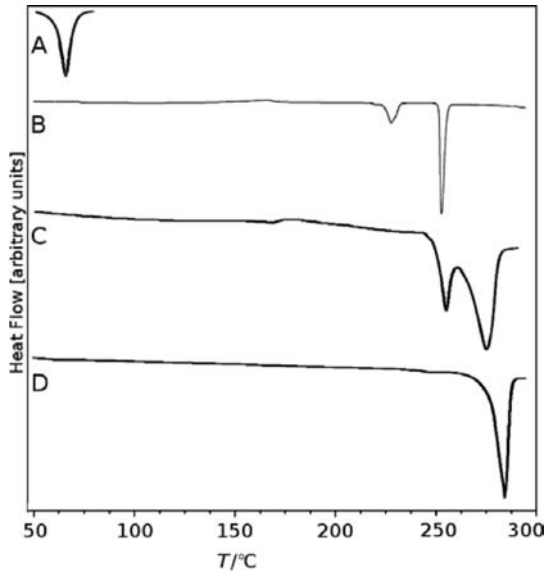

Figure 3. Differential scanning calorimetry of (A) neat **1**; (B) neat TPP-d_{12}; (C) 10%**1**@TPP-d_{12}; (D) 15%**1**@TPPd_{12}.

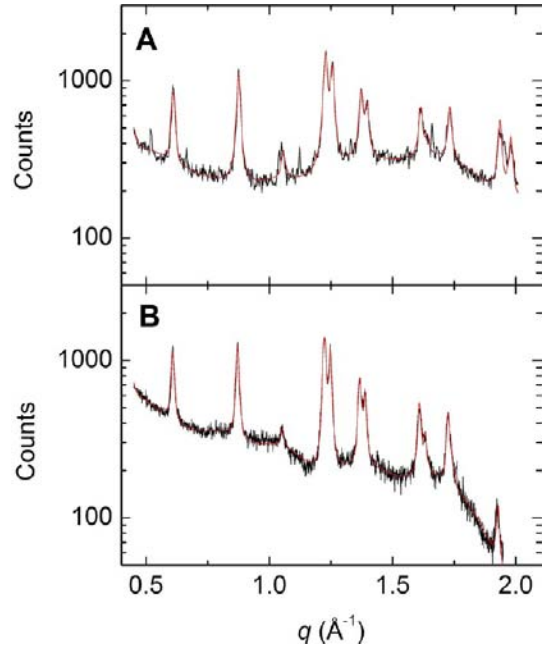

Figure 4. XRD results for (A) 10%**1**@TPP-d_{12} and (B) 15%**1**@TPP-d_{12}. Both materials are fitted (solid red lines) to a simple hexagonal structure consistent with the NMR data. 10%**1**@TPP-d_{12} shows minor impurity peaks of monoclinic TPP.

The DSC traces (Figure 3) show hexagonal TPP-d_{12} to behave nearly the same as hexagonal TPP[31,38] and are interpreted similarly. They start with a broad exotherm centered at ~148 °C, associated with the first-order transition of hexagonal TPP-d_{12} into its more stable monoclinic form. An endotherm at 222 °C is attributed to a first-order transition of monoclinic TPP-d_{12} into hexagonal TPP-d_{12}, and an endotherm at 252 °C to melting. The single endotherm of the neat rotor **1** at 62 °C corresponds to melting. The very broad exotherm in the DSC of 10%**1**@TPP-d_{12} (178 °C) is attributed to the first order transition of a minor excess of empty hexagonal TPP-d_{12} into its monoclinic form. The endotherms are due to the melting of excess pure TPP-d_{12} (255 °C) and of the inclusion compound (275 °C). The DSC trace of the inclusion compound 15%**1**@TPP-d_{12} shows a single endotherm at 284 °C, due to the congruent melting of the inclusion compound. The DSC trace of 8%**1**@TPP-d_{12} is similar to that of 10%**1**@TPP-d_{12}.

X-ray Powder Diffraction (Figure 4). The same samples that were used for solid-state NMR measurements were also used for copper Kα_1 wavelength X-ray powder diffraction measurements. Figure 4 shows the scattered X-ray photon counts versus the magnitude of the scattering wave vector q,

Table 1. Summary of the Solution NMR Assignments for 1

atom	^1H δ/ppm	^{13}C δ/ppm	atom	^1H δ/ppm	^{13}C δ/ppm	atom	^1H δ/ppm	^{13}C δ/ppm
a	7.36	130.83	e		131.46	i	1.66	38.08
b	7.02	126.54	f		135.82	j	1.08−1.31	29.27−32.10
c	7.53	130.8	g		80.03	k	1.08−1.31	22.87
d		134.27	h		85.54	l	0.88	14.29

dx.doi.org/10.1021/ja302173y | J. Am. Chem. Soc. 2012, 134, 10122−10131

related to scattering angle θ and X-ray wavelength λ by $q = 4\pi \sin \theta/\lambda$.

The trace for 10%**1**@TPP-d_{12} shows a sequence of diffraction peaks that fit a single hexagonal structure with lattice parameters that are expanded in the in-plane direction to 11.890 ± 0.002 Å and contracted in layer spacing to 10.080 ± 0.002 Å, and it also shows small impurity peaks at locations consistent with the monoclinic phase of TPP. The lattice parameters represent a 3.8% expansion and a 0.8% contraction, respectively, with respect to the 11.454 ± 0.005 Å and 10.160 ± 0.005 Å values reported for empty hexagonal TPP.[48] Peak widths suggest a typical powder particle size of 26 nm.

The trace for 15%**1**@TPP-d_{12} shows diffraction peaks that fit a single hexagonal structure with lattice parameters expanded in the in-plane direction to 11.934 ± 0.001 Å and contracted in layer spacing to 10.075 ± 0.001 Å. These values represent a 4.2% expansion and a 0.8% contraction. Peak widths suggest a powder particle size of 35 nm. No evidence is found of monoclinic TPP.

Solid-State ^{13}C CP MAS NMR of 1@TPP. The spectra of 10%**1**@TPP-d_{12} were recorded using t_C = 5 and 0.2 ms contact times (Figure 5). They are dominated by alkyl resonances in the aliphatic region and by three aromatic singlet resonances of the hexagonal TPP-d_{12} carbons that receive their magnetization from the protons of nearby guest molecules. The ^{13}C SPE MAS NMR spectrum recorded with 10 s recycle delay pinpointed the aromatic signals of **1**. The short contact time spectrum shows resonances from quaternary carbons (C_d, C_e, and C_f) decreased in intensity relative to those of the protonated carbons (C_a, C_b, and C_c) and was used to distinguish between them. The signals were tentatively assigned by comparison with the solution ^{13}C NMR spectrum (Figure 2A). The signals of the protonated carbons overlap with each other and partially with the central TPP-d_{12} signal at 124.4 ppm.

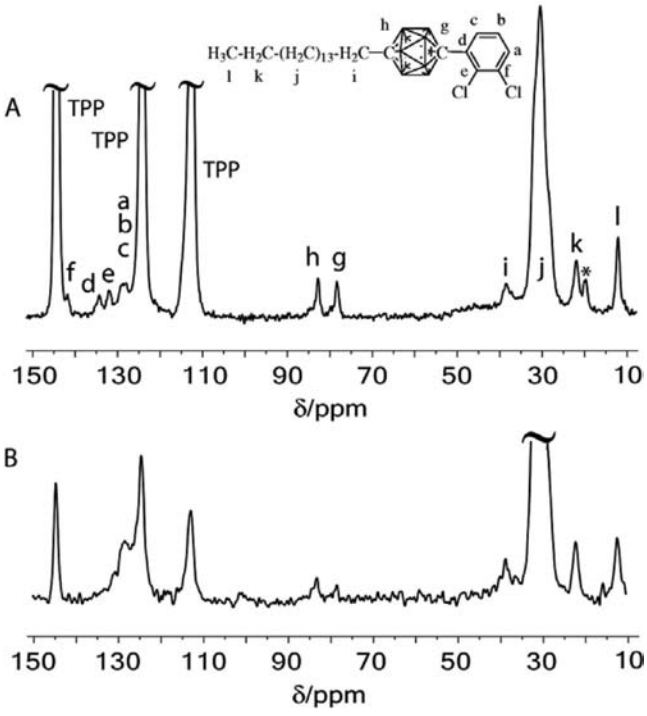

Figure 5. ^{13}C CP MAS NMR spectra of 10%**1**@TPP-d_{12}. (A) contact time t_C = 5 ms; (B) t_C = 0.2 ms.

Carbon C_f is shifted 4.1 ppm downfield relative to signal γ in the solid-state ^{13}C CP MAS NMR spectrum of neat **1** (Figure 2C), and 6.0 ppm downfield relative to the solution ^{13}C NMR spectrum. The carbon signal β in the solid-state ^{13}C NMR spectrum of neat **1** gives rise to two resolved resonances, C_d and C_e, in the spectrum of the inclusion compound 10%**1**@TPP-d_{12}. The signal C_d in the spectrum of 10%**1**@TPP-d_{12} is 0.6 ppm downfield from the peak β in the solid-state ^{13}C NMR spectrum of neat **1**, and 0.04 ppm relative to the solution ^{13}C NMR spectrum of **1**, which is within the resolution error of the solid-state ^{13}C NMR spectrum of 10%**1**@TPP-d_{12}. The signal C_e appears 1.3 ppm upfield from the β signal in the solid-state ^{13}C NMR spectrum of neat **1**, and it displays a small change in the chemical shift by +0.7 ppm relative to the solution ^{13}C spectrum of **1**. The protonated aromatic carbons C_a, C_b, and C_c are not resolved in the solid-state spectrum of either neat **1** or 10%**1**@TPP-d_{12}, and it is not possible to tell whether one of the carbon signals in the solid-state ^{13}C NMR spectrum of 10%**1**@TPP-d_{12} lies beneath the central carbon signal of TPP-d_{12}.

In the solid-state ^{13}C NMR spectrum of 10%**1**@TPP-d_{12}, the *p*-carborane signals C_g and C_h are shifted upfield relative to both the solution spectrum of **1** (C_g, 1.7 ppm; C_h, 2.7 ppm) and the solid state spectrum (both 2.4 ppm), and both display small downfield shoulders with chemical shifts similar to those in the ^{13}C NMR spectra of **1** as a solid and in solution. The aliphatic carbons C_i, C_j, C_k, and C_l all show an upfield change in the chemical shift by 1.3 to 3.3 ppm relative to the solid-state ^{13}C NMR spectrum of neat **1**. A comparison of the inclusion compound spectrum with the solution ^{13}C NMR spectrum of **1** shows an upfield change in the chemical shifts for the carbons C_k (0.9 ppm) and C_l (2.2 ppm) and a small downfield change for the carbons C_i (0.4 ppm) and C_j (1.0 ppm).

The solid-state ^{13}C CP MAS NMR spectra of the inclusion compounds 8%**1**@TPP-d_{12} (Figure 6A) and 10%**1**@TPP-d_{12} recorded with t_C = 5 ms (Figure 5A) show nearly identical sets of peaks. The variation of the chemical shift is within 0.1 ppm except for carbons C_h, C_g, and C_i, where the difference is −0.7 ppm for C_h and C_g and +0.3 ppm for C_i.

The solid-state ^{13}C CP MAS NMR of 15%**1**@TPP-d_{12} with t_C = 5 ms and solid-state ^{13}C SPE MAS NMR with a short relaxation delay (3 s) are shown in Figure 6. A comparison with the solid-state 10%**1**@TPP-d_{12} (Figure 5A) shows that the resolved quaternary carbons C_d and C_e and the protonated carbons C_a, C_b, and C_c have similar chemical shifts in all the inclusions of the rotor **1**. The signals in 15%**1**@TPP-d_{12} are broader. It is not obvious whether one of the carbon signals C_a, C_b, and C_c overlaps with the middle TPP-d_{12} carbon peak. The signal of carbon C_f has changed and is no longer resolved. The *p*-carborane and the aliphatic regions of the solid-state ^{13}C NMR spectra of 10%**1**@TPP-d_{12} and 15%**1**@TPP-d_{12} are very similar with only a small variation in chemical shifts. In the latter spectrum, the downfield shoulders of the *p*-carborane carbons C_g and C_h have higher relative intensity, suggesting that this more concentrated sample is more significantly heterogeneous. The signal of carbon C_i is broader, and the carbon C_k coincides with a spinning sideband in the spectrum of 15%**1**@TPP-d_{12}. In the solid-state ^{13}C SPE MAS NMR spectrum of 15%**1**@TPP-d_{12}, where the signals of fast relaxing carbons should be enhanced, all carbon signals of **1** are enhanced relative to those of TPP-d_{12}, and a new signal C_f is apparent. Additional weak downfield peaks of the *p*-carborane carbons C_g and C_h are detected, indicating that the sample is

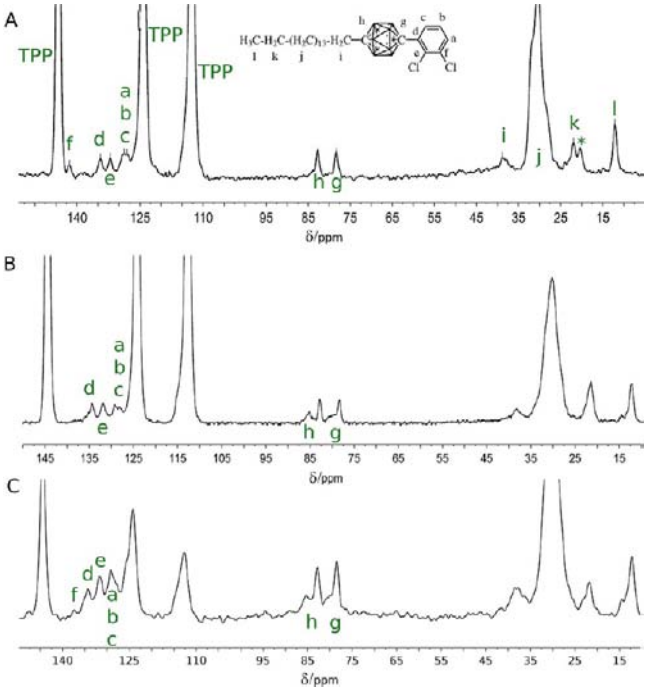

Figure 6. ^{13}C NMR of the inclusion compounds of **1** in TPP-d_{12}. (A) 8%**1**@TPP-d_{12} ^{13}C CP MAS; (B) 15%**1**@TPP-d_{12} ^{13}C CP MAS; (C) 15%**1**@TPP-d_{12} ^{13}C SPE MAS. The asterisk marks a spinning sideband.

heterogeneous and different *p*-carborane moieties experience distinct environments (Figure 6B).

Solid-State ^{31}P NMR of 1@TPP. The solid-state ^{31}P SPE and CP MAS NMR spectra of 10%**1**@TPP-d_{12} and 15%**1**@TPP-d_{12} all contain a single resonance at 34.2 ppm (Figure S3 in the Supporting Information).[38] The spectra of 8%**1**@TPP-d_{12} are similar.

Solid-State 2-D $^{1}H-^{13}C$ NMR of 1@TPP. Figure 7 shows solid-state 2-D $^{1}H-^{13}C$ heterocorrelated CP MAS NMR spectra of 10%**1**@TPP-d_{12} using Lee–Goldburg decoupling and 15 kHz spinning speed, performed at increasing $^{1}H-^{13}C$ cross-polarization times, allowing the magnetization to travel through space at increasingly longer distances.[49,50] At 0.1 ms cross-polarization time, only correlations of hydrogen nuclei at short distance from their bonded carbons are observed. The proton and carbon domains show greatly reduced spectral overlap and upfield shifts of about 2 ppm relative to the solution spectrum of **1** for the alkyl signals. At a contact time of 0.5 ms, correlations of alkyl protons with the TPP-d_{12} carbons are present in the spectrum. More $^{1}H-^{13}C$ host–guest correlations are observed at 1.25 ms and longer cross-polarization times. A remarkable upfield shift of 1.5 ppm relative to the solution spectrum is detected for the BH protons. No correlations of the rotator atoms with the TPP aromatic signals are observable even at longer cross-polarization times (2 ms).

Dielectric Spectroscopy. The results of dielectric loss measurements on the same samples of 10%**1**@TPP-d_{12} and 15%**1**@TPP-d_{12} that were used for NMR and X-ray diffraction studies are shown in Figure 8. Two distinct frequency-dependent dispersing loss peaks are observed for 10%**1**@TPP-d_{12}. The first peak is centered at ~150 K, and a much weaker structure is seen just below 100 K. A very low temperature dispersing structure and a rise in loss and

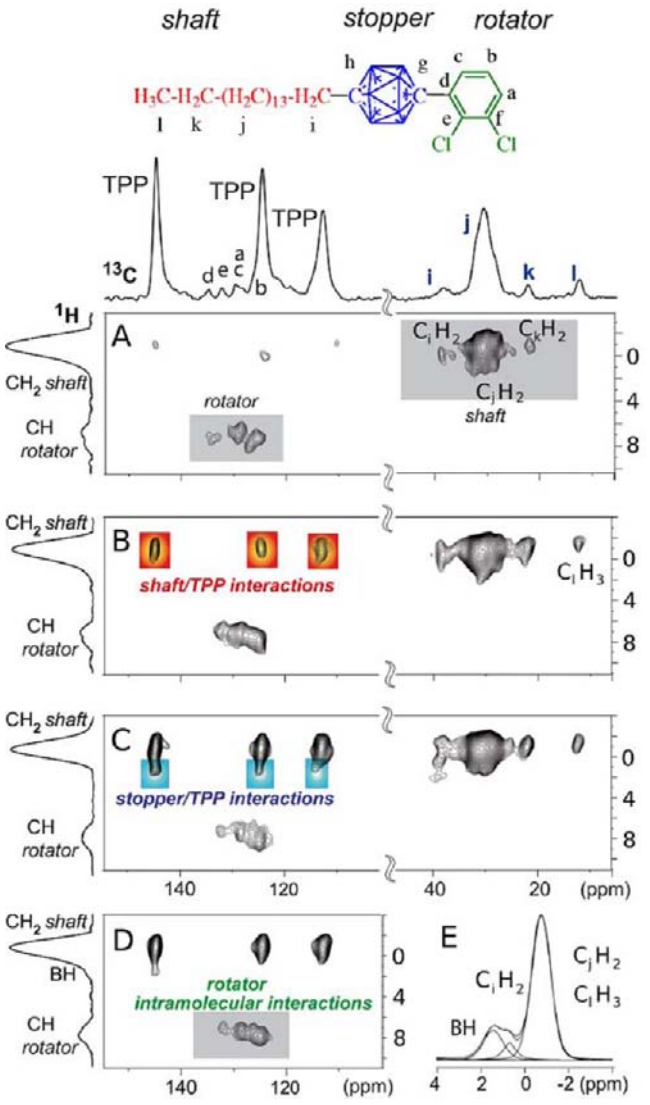

Figure 7. 2-D solid-state $^{1}H-^{13}C$ HETCOR NMR spectra of 10%**1**@TPP-d_{12} at cross-polarization times of (A) 0.1; (B) 0.5; (C) 1.25; and (D) 2 ms, using Lee–Goldburg decoupling and 15 kHz spinning rate. Intermolecular interactions of the alkyl and carborane moieties with the host are highlighted in orange and blue, respectively. (E) ^{1}H MAS NMR spectrum recorded at 600 MHz and spinning speed of 35 kHz.

dispersion above 250 K are both consistent with the behavior of the empty capacitor and arise from the silica substrate (see the discussion of the dielectric spectroscopy technique). The major 10%**1**@TPP-d_{12} loss peak is fitted to a rotational barrier height of 7.4 ± 0.8 kcal/mol, a barrier asymmetry parameter of 0.1 ± 0.05 kcal/mol, and a frequency factor of $(6 \pm 1) \times 10^{14}$ Hz. The smaller peak is fitted to a barrier height of 2.9 ± 0.3 kcal/mol, a barrier asymmetry parameter of 0.25 ± 0.05 kcal/mol, and a frequency factor of $(1.1 \pm 0.2) \times 10^{12}$ Hz.

In contrast, 15%**1**@TPP-d_{12} displays a very broad and dispersing loss structure that covers the entire temperature range from ~50 K to above 200 K. We extract a rough rotational barrier for the main peak of 4 ± 1 kcal/mol, and a frequency factor of $\sim 1 \times 10^{10}$ Hz. The lowest temperature edge of the loss structure disperses with frequency in a manner consistent with a barrier of 1.2 ± 0.4 kcal/mol.

Calculations. The B3LYP/TZVP method was used to calculate the dipole moment of 2,3-dichlorobenzene (2.64 D, in

dx.doi.org/10.1021/ja302173y | J. Am. Chem. Soc. 2012, 134, 10122–10131

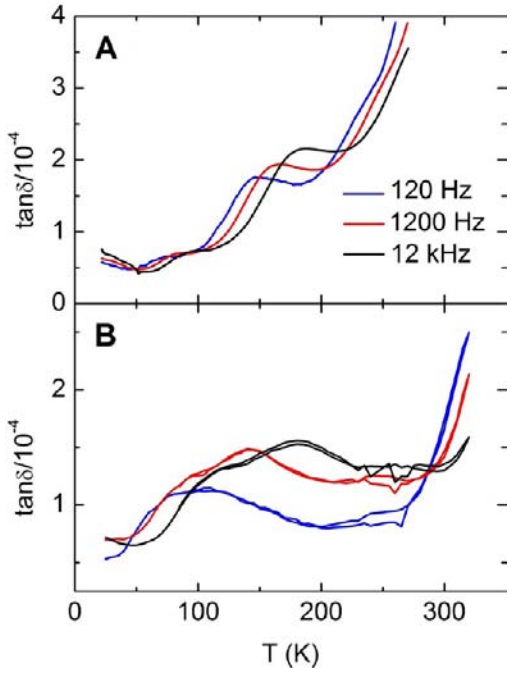

Figure 8. Dielectric losses versus temperature with measurement frequency as a parameter: (A) 10%**1**@TPP-d_{12}; (B) 15%**1**@TPP-d_{12}.

good agreement with the measured[51] value of 2.51 D) and the intrinsic rotational barrier of 2,3-dichlorophenyl against carborane in an isolated molecule of a model compound, 1-(2,3-dichlorophenyl)-*p*-carborane. A value of 1.56 kcal/mol was obtained for the difference between the energy of the lowest minimum and the energy of the transition state along the relaxed rotational coordinate.

DISCUSSION

Choice of Host. In addition to favorable spectroscopic properties, TPP offered a short channel-to-channel distance (~11.5 Å) and a suitable internal diameter, often quoted[32,35,52,53] as 4.5 or 4.6 Å. Using the experimental atomic positions in empty TPP[48] and Bondi[54] van der Waals radii, the diameter of a circle inscribed in the hexagonal cross section yields 4.8 Å. Van der Waals potentials are soft, with the channel walls adjusting somewhat to the steric demands of a guest,[55] and we use 4.5−5.0 Å as a rough guide. A further uncertainty is introduced by the "alternating triangle" hexagonal structure of TPP channels shown in Figure 1, which implies that this nominal limitation on guest diameter applies only when the guest is long and cylindrical. A short flat guest, such as an aromatic ring, will only need to fit into a triangular space, whose height is ~6.6 Å. Indeed, benzene (~6.7 Å diameter) enters TPP channels readily.[30] Thus, a stopper may stay imbedded in the very top layer of the TPP solid rather than located outside the solid surface, and can still prevent further insertion of a shaft into bulk TPP.

Choice of Guest. For the formation of a surface inclusion compound, we need a shaft with a high affinity for entering the TPP channel, a much larger stopper that would refuse to enter, and a dipolar rotator large enough to avoid backward (rotator first) entry. The terminal bond of the shaft, which defines the orientation of the stopper and thus the direction of the rotator axis, should ideally be perpendicular to the surface.

Many types of straight molecular rods[56] might serve as shafts. Obvious initial concerns are assuring sufficient affinity for the channel and a sufficient difference between the diameters of the shaft and of the stopper, without which the shaft might stretch the channel enough for the stopper to enter as well. We have chosen an alkyl chain that is long and narrow, since alkanes are known to enter TPP channels eagerly.[36,37,40,41,53] The price to pay is that the direction of its terminal bond will most likely deviate from the surface normal. The choice of *p*-carborane as a stopper was based on its large diameter (~7.6 Å[57]) and the ease with which its antiparallel axial CH bonds can be substituted. The choice of *o*-dichlorophenyl as the rotator was based on the significant dipole moment of *o*-dichlorobenzene (2.51 D[51]) and its large transverse size (~7.8 Å[58]).

The synthesis of **1** was straightforward. The Ulmann conditions for the coupling of *p*-carborane to an arene[59] appear to be applicable generally for this type of rotor shaft, whereas the more popular Pd-catalyzed coupling produced large quantities of 1,2-dichlorobenzene, presumably due to slow transmetalation of the cuprous *p*-carborane salt with an arylpalladium halide.

Evidence for the Formation of a Surface Inclusion Compound. The NMR evidence, along with all the other results, leaves no doubt that we have formed the desired surface inclusion compound of **1** in TPP microcrystals, with the shaft and the stopper inserted to various degrees into the TPP channels and the rotator outside the surface (Figure 9). In the following, we present our arguments.

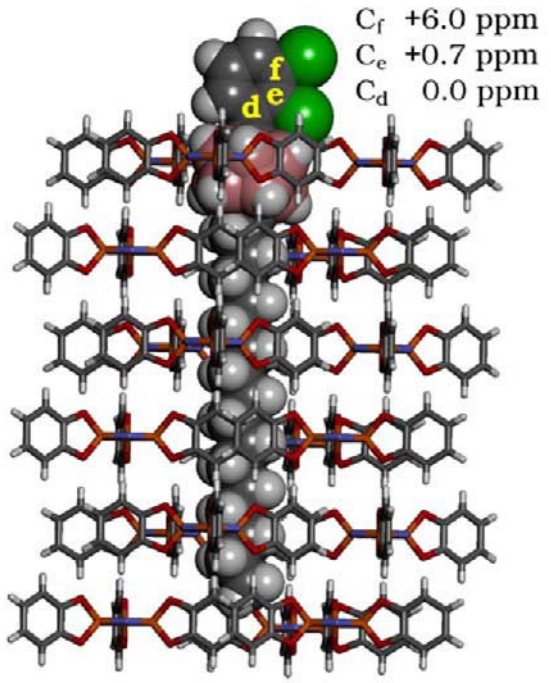

Figure 9. Qualitative picture of the extent of insertion of rotor **1** into a TPP channel.

DSC and X-ray Diffraction. The results of these two methods for 10%**1**@TPP-d_{12} and 15%**1**@TPP-d_{12} fit the formation of a hexagonal inclusion compound. The two samples differ in that all the TPP molecules are present within the inclusion compound in 15%**1**@TPP-d_{12}, while in 10%**1**@TPP-d_{12} excess TPP is left as the monoclinic phase, suggesting that all the guest molecules **1** participate in the formation of the

dx.doi.org/10.1021/ja302173y | J. Am. Chem. Soc. 2012, 134, 10122−10131

inclusion compound. The observed increase in the in-plane lattice parameter with increased rotor concentration and an associated increase in the estimated powder particle size indicate how much the TPP channels have changed as a result of the insertion of a guest molecule. The nominal internal van der Waals channel diameter is now ∼5.3 Å instead of ∼4.95 Å, somewhat closer to the ∼6.7 Å value for the benzene ring, but still much smaller than the diameters of *p*-carborane and 1,2-dichlorobenzene. This is consistent with these components of the rotor molecules remaining localized in the surface of thin platelet-shaped microcrystals.

NMR Spectroscopy. Detailed information on the local structure of the inclusion compounds **1**@TPP resulted from solid-state NMR measurements and relies on the unambiguous assignment of peaks in the solution spectrum of **1**. There are two primary causes of differences between the solution NMR of **1** and its solid NMR, neat or in **1**@TPP.

(i) First, a flexible guest in an inclusion compound generally experiences a limited conformational interconversion, since alkane chains inside TPP are much more spatially constrained to the all-anti conformation.[37,40,60] The motion is typically fast on the NMR time scale at room temperature.[34,39,40,61] The solid-state NMR spectra of **1**@TPP are therefore averaged over the accessible alkyl conformations, but differently than in solution.[37,40] The aromatic carbon signals in the neat solid **1** or in **1**@TPP are not likely to be affected much by conformational effects (rotation about the C_g-C_d bond).

(ii) Second, the solid spectra are affected by the local shielding and deshielding effects due to neighboring molecules. In a crystal of neat **1**, these will result primarily from π-stacking interactions and cannot be elucidated without the knowledge of crystal packing. In our case, the effects on the chemical shifts of the aromatic carbons are comparable to their peak separation, and we cannot make reliable aromatic carbon assignments based on the solution chemical shifts. The resolved aliphatic and *p*-carborane carbon signals are separated sufficiently for the assignments to be made confidently.

The situation is much more favorable in the more important case of **1**@TPP. There is a shielding environment inside the TPP channel and a deshielding environment at the crystal surface close to the channel ends, due to the magnetic susceptibility of the aromatic rings of TPP that line the channel walls. The effect was observed on several inclusion compounds of TPP[37,40] and confirmed by ab initio HF-GIAO calculations.[43]

The solid-state ^{13}C CP MAS NMR spectra of 8%**1**@TPP-d_{12} (Figure 6), 10%**1**@TPP-d_{12} (Figure 5), and 15%**1**@TPP-d_{12} (Figure 6) are dominated by three aromatic singlets due to hexagonal TPP-d_{12}. The fact that the TPP-d_{12} carbons are being cross-polarized demonstrates that at least some of the guest compound **1** is inserted. The solid-state ^{31}P CP MAS NMR spectra (Supporting Information Figure S3) confirm the hexagonal structure and the insertion of **1**. These spectra provide no information about the local structure of any fraction of TPP-d_{12} that does not contain inserted **1**, but the solid-state ^{31}P SPE MAS NMR spectra of 10%**1**@TPP-d_{12} and 15%**1**@TPP-d_{12} (Figure S3) reveal that the structure is hexagonal in nearly the entire sample, in agreement with the evidence from X-ray diffraction.

^{1}H−^{13}C 2-D heterocorrelated experiments are a rich source of information, as long as the hydrogen domain shows enough resolution to distinguish hydrogen resonances due to different groups. This is not easily achieved, given the line broadening caused by the strong dipolar coupling among proximate hydrogens. Several homonuclear decoupling pulse sequences and extremely high spinning speeds can remove diffuse coupling and minimize line widths, but the fast spinning rates hamper cross-polarization. We succeeded with Lee−Goldburg decoupling and 15 kHz spinning speed. The 2-D results on 10%**1**@TPP-d_{12} provide independent information on the degree of insertion of the molecules of **1** into the TPP channels and on the effectiveness of the spontaneous host−guest self-assembly.

Location of the Rotator in 1@TPP-d_{12}. The similarity of the pattern of the resolved ^{13}C NMR aromatic signals of **1** in the solid inclusion compounds **1**@TPP-d_{12} and in solution is remarkable and permits an assignment of the aromatic signals, in agreement with the short contact time solid-state ^{13}C CP MAS NMR spectrum of 10%**1**@TPP-d_{12} (Figure 5B), which discriminates between the protonated and quaternary carbons.

Several features of the spectra of 8%**1**@TPP-d_{12} and 10%**1**@TPP-d_{12} provide compelling evidence that the rotator protrudes outside the TPP channel: (i) The absence of any substantial displacements of the chemical shifts in the hydrogen domain in the 2-D MAS NMR spectrum, which should be very sensitive in view of the total spectral range. In fact, the aromatic protons resonate at δ_H = 6.8−7.3 ppm, just as in isolated **1**. (ii) The absence of any correlations of the rotator atoms with the aromatic signals of the TPP host, even at cross-polarization times as long as 2 ms (Figure 7D). (iii) The large 4.1 ppm downfield displacement of the C_f chemical shift relative to the spectrum of neat **1** (6.0 ppm relative to the solution spectrum of **1**), given that the inside of the channel only imposes a shielding environment.[32,37,39−43] The protonated carbon C_b should find itself in a similar deshielding environment, but it is not seen due to signal overlap. (iv) The near absence of any change in the chemical shift of C_d, suggesting that it is located at the boundary of the shielding and deshielding zones, and the 0.7 ppm downfield change in the chemical shift of carbon C_e. The gradual change of the anisotropic magnetic susceptibility experienced by these carbons is in good agreement with signal assignments.

The solid-state ^{13}C NMR spectra of 15%**1**@TPP-d_{12} are similar but show more heterogeneity, as judged by the larger downfield shoulders on the peaks of C_g and C_h. The aromatic region is different than in the spectra of 8%**1**@TPP-d_{12} and 10%**1**@TPP-d_{12}, mainly in that the signal of carbon C_f is absent. This could be caused by the heterogeneity of the sample. Figure 9 shows that a small displacement in the vertical position of the guest near a channel end can cause a large change in the chemical shift. The channels in the inclusion compound 15%**1**@TPP-d_{12} are saturated, and it is likely that many different degrees of insertion are present, providing different shielding environments.

The absolute magnitude of the 6.0 ppm displacement of the chemical shift of C_f exceeds those known from the shielding inside TPP channels. This is understandable when one considers that in the bulk the shielding in any one layer is counteracted by deshielding provided by adjacent layers, but at the surface this effect is absent. The magnitudes of the displacement for the various atoms located in the rotator follow a logical sequence as a function of their distance from the surface when one allows for averaging due to the rotation of the rotator.

Location of the Shaft. Several pieces of convincing evidence demonstrate that the hexadecyl group is included in

TPP-d_{12}: (i) Upfield ^{1}H shifts of about 2 ppm relative to the solution spectrum of **1** are observed for the signals of shaft atoms, even resulting in a negative proton chemical shift value, $\delta_H(C_j) = -0.8$ ppm (Figure 7E). Such large magnetic susceptibility effects can only occur upon close-contact arrangement of the alkyl methylene groups, facilitated by multiple CH−π interactions between the host and guest.[40−43] (ii) At 0.5 ms contact times (Figure 7B), the correlations of alkyl hydrogens with TPP-d_{12} carbons are clearly detected, confirming the close host−guest proximity. (iii) The chemical shifts of aliphatic carbons C_i, C_j, C_k, and C_l in the solid-state ^{13}C NMR spectra of **1**@TPP relative to solution are moved upfield. The smaller size of these changes is due to the higher conformational freedom of the aliphatic chain in the solution compared to the inside of the channel, where they are mostly all-anti,[37,40,60] generating a shift opposed to that of the magnetic susceptibility effect.

Location of the Stopper. Like the shaft, the stopper is inserted into TPP-d_{12}: (i) The carborane proton chemical shift has a remarkable value of $\delta_H = 1.5$ ppm. These hydrogens were clearly detected in the 1-D ^{1}H MAS spectrum at 600 MHz and 35 kHz (Figure 7E). (ii) The ^{1}H−^{13}C host−guest correlations of the *p*-carborane with TPP-d_{12} can be observed at 1.25 ms cross-polarization times (Figure 7C). (iii) The ^{13}C chemical shifts of C_g and C_h are displaced upfield from the solution spectrum by 1.7 and 2.1 ppm, respectively (Figure 5A).

Since the *p*-carborane diameter fits into the triangular 6.7 Å niche of three TPP paddles but exceeds the 5.04 Å height of the prismatic boxes in the TPP channels (Figure 1), the *p*-carborane moieties must reside in the top TPP layer at the (001) crystal surface, where they feel a large magnetic susceptibility effect. Only a small fraction of the *p*-carborane stoppers is not inserted, as demonstrated by the downfield shoulder in the signal of these two carbons. The shoulder increases with higher loading of the rotor **1** in TPP-d_{12}.

Integrating all the NMR information, we conclude that the rotor guest **1** forms a surface inclusion in the TPP host at the geometry shown qualitatively in Figure 9.

Rotation: Dielectric Spectroscopy. Information on the actual performance of the inserted rotors was provided by dielectric spectroscopy. The rotation of a dipole moment, such as the rotators in our inclusion compounds, makes a contribution to the dielectric signal by aligning with the applied electric field in the capacitor. For a dipole that moves in a rotational potential energy surface with specified energy barriers between wells, the contribution to the dielectric response becomes temperature dependent. At high temperatures, dipoles are easily thermally activated over the energy barriers and are largely free to align with the applied field. At low temperatures, dipoles are trapped in potential wells. At an intermediate temperature, where the measurement frequency is equal to the rate of thermal activation, the motion lags the electric field and contributes to dielectric loss. Thus, dielectric loss spectroscopy typically yields loss peaks at temperatures where the measurement frequency is equal to a thermal activation rate, and the temperature dependence of the peak intensity provides information about the asymmetry parameter, i.e. the energy difference between the wells on both sides of the barrier to rotation. Measurements taken at different frequencies and temperatures can thus be used to measure rotational barriers E_b, attempt frequencies A, and asymmetry parameters s (cf. Supporting Information).[3,11]

The dielectric spectra confirm the conclusions from NMR: 10%**1**@TPP-d_{12}, with its more uniform NMR peak shapes, is also found to produce a more uniform dielectric spectrum. We find only two dispersing peaks, consistent with only two rotational barriers. Both observed barriers are significantly higher than the 1.6 kcal/mol rotational barrier calculated for the isolated molecule. The peak at roughly 150 K with a rotational barrier of 7.4 kcal/mol accounts for roughly three times more loss than is found for the 2.9 kcal/mol peak near 100 K, and it corresponds to a majority of the rotators. While the rotator is certainly outside the channel, the downfield shifts of its aromatic carbons indicate that it is close enough to the channel end for interactions with the local TPP environment. We propose that the observed barriers are due to the interactions of the rotator with the TPP surface during the turning motion. Most of the rotor molecules are inserted deeply (Figure 9), with the dichlorophenyl rotator rubbing the TPP surface and generating the higher barrier, and a minority are inserted less deeply, with the rotator touching the surface only lightly. It is likely that the rotator axis is not normal to the surface but is tilted to accommodate the direction of the bond that attaches the alkyl chain to the carborane carbon, and this tilt brings the chlorine substituents on the rotator closer to the TPP surface and may well be helping the stopper to perform its function.

In contrast, 15%**1**@TPP-d_{12} shows significantly more heterogeneity in its NMR peaks and also in its dielectric loss peaks. Increased variability in the local environment is apparently leading to a broader range of rotational barriers. The dispersion at temperatures above 200 K is consistent with rotational barriers as high as 9 kcal/mol, suggesting that in the densely packed environment the rotators of some molecules may interfere with their neighbors in nearby channels, which would be possible if the rotator axes are indeed tilted as we suspect. The low-temperature edge of the dielectric loss curve observed near 50 K disperses in a manner consistent with a rotational barrier of 1.2 ± 0.4 kcal/mol, a value close to the calculated intrinsic rotational barrier of the isolated molecule. This low barrier presumably corresponds to rotor molecules whose rotator protrudes well above the TPP surface and does not interfere with neighbors.

■ CONCLUSIONS

Rotor **1** forms a surface inclusion compound with TPP-d_{12}, with the *n*-hexadecyl chain and *p*-carborane inserted in the channel and the 2,3-dichlorophenyl rotator protruding above the surface of the crystal. This has been shown by a combination of solid-state NMR spectroscopy, differential scanning calorimetry, X-ray powder diffraction, and dielectric spectroscopy. The inclusion compounds show increasing heterogeneity and a range of barrier heights as the loading of the rotor **1** in TPP-d_{12} is augmented.

We conclude that structures of type **1** are suitable for producing a surface inclusion compound with TPP but exhibit barriers to rotation that are higher than desired, presumably because the rotator axes are tilted and the chlorine atoms hit the surface as the rotator turns. It will be interesting to examine structures in which the alkyl chain is replaced by a shaft that favors a direction of rotator axle that is normal to the surface, in the hope that they will possess lower barriers to rotation.

■ METHODS AND PROCEDURES

The procedures used to synthesize **1**, **TPP-d_{12}**, and **1@TPP-d_{12}** and to perform measurements on them, and the computer program used for

barrier height calculation in a model system are described in the Supporting Information.

■ ASSOCIATED CONTENT

Supporting Information

Methods of synthesis, measurement, and computation; assignment of solution NMR spectrum; and Figures S1−S3. This material is available free of charge via the Internet at http://pubs.acs.org.

■ AUTHOR INFORMATION

Corresponding Author

michl@eefus.colorado.edu

Notes

The authors declare no competing financial interest.

■ ACKNOWLEDGMENTS

The research leading to these results has received funding from the European Research Council (FP7/2007-2013/ERC Grant 227756), from the U.S. National Science Foundation (CHE 0848663 and Materials Research Science and Engineering Centers Grant No. DMR-0820579) and from the Lombardy Region, Italy.

■ REFERENCES

(1) Kottas, G. S.; Clarke, L. I.; Horinek, D.; Michl, J. *Chem. Rev.* **2005**, *105*, 1281.
(2) Khuong, T.-A. V.; Nunez, J. E.; Godinez, C. E.; Garcia-Garibay, M. A. *Acc. Chem. Res.* **2006**, *39*, 413.
(3) Horansky, R. D.; Magnera, T. F.; Price, J. C.; Michl, J. In *Controlled Nanoscale Motion*; Lecture Notes in Physics, Vol. *711*; Linke, H., Månsson, A., Eds.; Springer: Berlin and Heidelberg, 2007; p 303.
(4) Crowly, J. D.; Kay, E. R.; Leigh, D. A. *Intell. Mater.* **2008**, 1.
(5) Garcia-Garibay, M. A. *Nat. Mater.* **2008**, *7*, 431.
(6) Michl, J.; Sykes, E. C. H. *ACS Nano* **2009**, *3*, 1042.
(7) Augulis, R.; Klok, M.; Feringa, B. L. *Phys. Status Solidi C* **2009**, *6*, 181.
(8) Dominiguez, Z.; Dang, H.; Strouse, M. J.; Garcia-Garibay, M. A. *J. Am. Chem. Soc.* **2002**, *124*, 2398.
(9) Rodriguez-Molina, B.; Ochoa, M. E.; Farfan, N.; Santillan, R.; Garcia-Garibay, M. A. *J. Org. Lett.* **2009**, *74*, 8554.
(10) Karlen, S. D.; Reyes, H.; Taylor, R. E.; Khan, S. I.; Hawthorne, M. F.; Garcia-Garibay, M. A. *Proc. Natl. Acad. Sci. U.S.A.* **2010**, *107*, 14973.
(11) Winston, E. B.; Lowell, P. J.; Vacek, J.; Chocholoušová, J.; Michl, J.; Price, J. C. *Phys. Chem. Chem. Phys.* **2008**, *10*, 5188.
(12) Gould, S. L.; Tranchemontagne, D.; Yaghi, O. M.; Garcia-Garibay, M. A. *J. Am. Chem. Soc.* **2008**, *130*, 3246.
(13) Lemouchi, C.; Vogelsberg, C. S.; Zorina, L.; Simonov, S.; Batail, P.; Brown, S.; Garcia-Garibay, M. A. *J. Am. Chem. Soc.* **2011**, *133*, 6371.
(14) Gimzewski, J. K.; Joachhim, C.; Schlitter, R. R.; Langlias, V.; Tang, H.; Johannsen, I. *Science* **1998**, *281*, 531.
(15) Stipe, B. C.; Rezaei, M. A.; Ho, W. *Science* **1998**, *279*, 1907.
(16) Rao, B. V.; Kwon, K.-Y.; Liu, A.; Bartels, L. *J. Chem. Phys.* **2003**, *119*, 10879.
(17) Sainoo, Y.; Kim, Y.; Komeda, T.; Kawai, M.; Shigekawa, H. *Surf. Sci.* **2003**, *536*, L403.
(18) Delden, R. A.; ter Wiel, M. K. J.; Pollard, M. M.; Vicario, J.; Koumura, N.; Feringa, B. L. *Nature* **2005**, *437*, 1337.
(19) Tierney, H. L.; Murphy, C. J.; Jewell, A. D.; Baber, A. E.; Iski, E. V.; Khodaverdian, H. Y.; McGuire, A. F.; Klebanov, N.; Sykes, E. C. H. *Nature Nanotechnol.* **2011**, *6*, 625.
(20) Zheng, X.; Mulcahy, M. E.; Horinek, D.; Galeotti, F.; Magnera, T. F.; Michl, J. *J. Am. Chem. Soc.* **2004**, *126*, 4540.
(21) Clarke, L. I.; Horinek, D.; Kottas, G. S.; Varaksa, N.; Magnera, T. F.; Hinderer, T. P.; Horansky, R. D.; Michl, J.; Price, J. C. *Nanotechnology* **2002**, *13*, 533.
(22) Eelkema, R.; Pollard, M. M.; Vicario, J.; Katsonis, N.; Ramon, B. S.; Bastiaansen, C. W. M.; Broer, D. J.; Feringa, B. L. *Nature* **2006**, *440*, 163.
(23) Pollard, M. M.; Lubomska, M.; Rudolf, P.; Feringa, B. L. *Angew. Chem., Int. Ed.* **2007**, *46*, 1278.
(24) Carroll, G. T.; Pollard, M. M.; van Delden, R.; Feringa, B. L. *Chem. Sci.* **2010**, *1*, 97.
(25) O'Brien, Z. J.; Karlen, S. D.; Khan, S.; Garcia-Garibay, M. A. *J. Org. Chem.* **2010**, *75*, 2482.
(26) Rodriguez-Molina, B.; Farfan, N.; Romero, M.; Mendez-Stivalet, J. M.; Santillan, R.; Garcia-Garibay, M. A. *J. Am. Chem. Soc.* **2011**, *133*, 7280.
(27) Mulcahy, M. E.; Magnera, T. F.; Michl, J. *J. Phys. Chem. C* **2009**, *113*, 20698.
(28) Horansky, R. D.; Clarke, L. I.; Winston, E. B.; Price, J. C.; Karlen, S. D.; Jarowski, P. D.; Santillan, R.; Garcia-Garibay, M. A. *Phys. Rev. B* **2006**, *74*, 054306.
(29) Rozenbaum, V. M.; Ogenko, V. M.; Chuiko, A. A. *Phys.-Usp.* **1991**, *34*, 883.
(30) Allcock, H. R.; Siegel, L. A. *J. Am. Chem. Soc.* **1964**, *86*, 5140.
(31) Sozzani, P.; Comotti, A.; Simonutti, R.; Meersmann, T.; Logan, J. W.; Pines, A. *Angew. Chem., Int. Ed.* **2000**, *39*, 2695.
(32) Sozzani, P.; Bracco, S.; Comotti, A.; Ferretti, L.; Simonutti, R. *Angew. Chem., Int. Ed.* **2005**, *44*, 1816.
(33) Meersmann, T.; Logan, J. W.; Simonutti, R.; Caldarelli, S.; Sozzani, P.; Comotti, A.; Kaiser, L.; Pines, A. *J. Phys. Chem. A* **2000**, *104*, 11665.
(34) Meitrovitch, E.; Belsky, I.; Vega, S. *J. Phys. Chem.* **1984**, *88*, 1522.
(35) Allcock, H. R.; Levin, M. L.; Whittle, R. R. *Inorg. Chem.* **1986**, *25*, 41.
(36) Primrose, A. P.; Parvez, M.; Allcock, H. R. *Macromolecules* **1997**, *30*, 670.
(37) Comotti, A.; Simonutti, R.; Catel, G.; Sozzani, P. *Chem. Mater.* **1999**, *11*, 1476.
(38) Comotti, A.; Simonutti, R.; Stramare, S.; Sozzani, P. *Nanotechnology* **1999**, *10*, 70.
(39) Brustolon, M.; Barbon, A.; Bortolus, M.; Maniero, A. L.; Sozzani, P.; Comotti, A.; Simonutti, R. *J. Am. Chem. Soc.* **2004**, *126*, 15512.
(40) Sozzani, P.; Comotti, A.; Bracco, S.; Simonutti, R. *Chem. Commun.* **2004**, 768.
(41) Sozzani, P.; Comotti, A.; Bracco, S.; Simonutti, R. *Angew. Chem., Int. Ed.* **2004**, *43*, 2792.
(42) Bracco, S.; Comotti, A.; Valsesia, P.; Beretta, M.; Sozzani, P. *Cryst. Eng. Commun.* **2010**, *12*, 2318.
(43) Bracco, S.; Comotti, A.; Ferretti, L.; Sozzani, P. *J. Am. Chem. Soc.* **2011**, *133*, 8982.
(44) Herzog, A.; Knobler, C. B.; Hawthorne, M. F.; Maderna, A.; Siebert, W. *J. Org. Chem.* **1999**, *64*, 1045.
(45) Ito, N.; Esaki, H.; Maesawa, T.; Imamiya, E.; Maegawa, T.; Sajiki, H. *Bull. Chem. Soc. Jpn.* **2008**, *81*, 278.
(46) Allcock, H. R. *J. Am. Chem. Soc.* **1963**, *85*, 4050.
(47) Tonelli, A. *NMR Spectroscopy and Polymer Microstructure: The Conformational Connection*; VCH Publishers: Deerfeld Beach, 1988.
(48) Comotti, A.; Bracco, S.; Ferretti, L.; Mauri, M.; Simonutti, R.; Sozzani, P. *Chem. Commun.* **2007**, 350.
(49) Vinogradov, E.; Madhu, P. K.; Vega, S. *Chem. Phys. Lett.* **1999**, *314*, 443.
(50) Sozzani, P.; Bracco, S.; Comotti, A.; Simonutti, R.; Camurati, I. *J. Am. Chem. Soc.* **2003**, *125*, 12881.
(51) Hurdis, E. C.; Smyth, C. P. *J. Am. Chem. Soc.* **1942**, *64*, 2212.
(52) Becker, P.; Comotti, A.; Simonutti, R.; Sozzani, P.; Saalwachter, K. *J. Phys. Chem. B* **2005**, *109*, 23285.
(53) Sozzani, P.; Bracco, S.; Comotti, A.; Simonutti, R. *Adv. Polym. Sci.* **2005**, *181*, 153.

(54) Bondi, A. *J. Phys. Chem.* **1964**, *68*, 441.
(55) Allcock, H. R.; Allen, R. W.; Bissell, E. C.; Smeltz, L. A.; Teeter, M. *J. Am. Chem. Soc.* **1976**, *98*, 5120.
(56) Schwab, P. F. H.; Levin, M. D.; Michl, J. *Chem. Rev.* **1999**, *99*, 1863.
(57) Bohn, R. K.; Bohn, M. D. *Inorg. Chem.* **1971**, *10*, 350.
(58) Masao, O.; Mariko, U.; Masahiko, A.; Junko, Y.; Ichiro, Y. *J. Mol. Struct.* **1986**, *147*, 77.
(59) Schöberl, U.; Magnera, T. F.; Harrison, R.; Fleischer, F.; Pflug, J. L.; Schwab, P. F. H.; Meng, X.; Lipiak, D.; Noll, B. C.; Allured, V. S.; Rudalevige, T.; Lee, S.; Michl, J. *J. Am. Chem. Soc.* **1997**, *119*, 3907.
(60) Sozzani, P.; Bovey, F. A.; Schilling, F. C. *Macromolecules* **1991**, *24*, 6764.
(61) Meitrovitch, E. *J. Phys. Chem.* **1984**, *88*, 6411.